IEEE TRANSACTIONS ON
AUTOMATION SCIENCE AND ENGINEERING

IEEE Xplore® Digital Library
http://ieeexplore.ieee.org/Xplore

Stability and Control of a Rider-Bicycle System: Analysis and Experiments

Pengcheng Wang, *Student Member, IEEE*, Jingang Yi, *Senior Member, IEEE*, and Tao Liu, *Senior Member, IEEE*

***Abstract*—We present stability and control analysis of a rider-bicycle system under human steering and body movements. The dynamic model of rider-bicycle interactions is first constructed to integrate the rider's body movement with the moving bicycle platform. We then present a human balance control strategies based on human riding experiments. The closed-loop system stability is analyzed and discussed. Quantitative influences of the bicycle physical parameters, the human control gains and the time delays are also analyzed and discussed. Extensive experiments are conducted to validate the human control models and demonstrate human balance performance using the bikebot, an instrumented bicycle platform. The presented modeling and analysis results can be potentially used for further development of bicycle-assisted rehabilitation for postural balance patients.**

***Note to Practioners*—Understanding human balance and control of bicycles is crucial for not only designing bicycle-based rehabilitation devices but also studying physical human-machine interactions for healthcare automation. This paper takes the rider and bicycle as an example of physical human-machine interactions to understand how human use their limbs and body movement to stabilize an unstable platform (i.e., bicycles.) We develop an instrumented bicycle system, called bikebot, to conduct human riding experiments. Using experimental data, we build the dynamic models for human steering and leaning control actions. Using these actuation models, stability analyses are conducted for rider-bicycle interactions and then validated by experiments. We also obtain the stability results by perturbing human visual and sensorimotor feedback. These results reveal that the visual feedback and the time delay in sensorimotor feedback mechanism play critical roles in stabilizing the unstable bicycle platform.**

***Index Terms*—Underactuated systems, human-robot interactions, balance stability, cycling, time-delay systems**

I. Introduction

HUMAN balance capability is crucial for many motor skills, such as standing, walking and running, etc. Human physiological delays often exist in sensorimotor feedback and therefore, increase complexity in analyzing these human balancing skills. Although many advances have been witnessed in recent years towards understanding human balancing tasks such as stick balancing [1], [2], quiet stance [3]–[5], balancing board [6], etc., few studies have been reported in human-machine interactions in which human full-body movements play an important role in balancing the entire systems. In this paper, we take an example of rider-bicycle systems to present stability and control analysis of these human-in-the-loop balance systems.

Recent clinical studies report that some Parkinson's disease patients who cannot maintain a stance balance and walking balance are able to freely ride bicycles [7], [8]. Bicycle is also considered as a potential postural balance rehabilitation device [9], [10]. Intrinsically unstable bicycles offer a unique platform to study fundamental principles of coupled physical human-machine interactions. Although bicycle dynamics and stability have been studied for a long time (e.g., [11]–[14]), few studies and experiments are reported to quantify the human balance mechanisms and performance [15]. The goal of this work is to present the stability and control analysis and experiments of the rider-bicycle system.

Rider's balance control mechanism is a combination of perception, decision and manipulation. Neuro-balance control models are reported in literature for human quiet stance. For example, the model in [3], [16] describes a human feedback mechanism of upper-body upright stance with the identified sensorimotor contributions. The model captures the human sensory responses to environment as short-, medium- and long-latency phasic mechanisms due to proprioception, vestibular and visual sensory, respectively. Using this neuro-control model, balance control stability analysis is conducted for riding stationary bicycles [17], [18]. Built on the work in [19], a rider steering model is presented in [20] for bicycle balancing and path-following tasks. Comparing with the work in [19], [20], the neuro-balance model in [3], [16] includes the human musculoskeletal characteristics such as body movements and time delays, which are important for bicycle riding. This model also captures various human sensorimotor properties and has been further validated through various stance balance experiments. Although qualitative discussions about balance mechanism are presented in [21], [22], no detailed, quantitative stability results of the rider-bicycle system are reported and demonstrated.

The work presented in this paper complements and extends the above-mentioned human-bicycle balance control analysis and experiments. We develop new models for the rider steering and body movement control strategies. Using these models, we then analyze stability and performance of the rider-bicycle system. The rider-bicycle dynamic model in this paper is built on and extended by the work of [23]. A proportional-derivative

The preliminary version of this paper was presented in part at the 2015 American Control Conference, July 1-3, 2015, Chicago, IL, USA. This work was supported in part by the US National Science Foundation under award CMMI-1334389. (*Corresponding author: J. Yi.*)

P. Wang was with the Department of Mechanical and Aerospace Engineering, Rutgers University, Piscataway, NJ 08854 USA. He is now with the Innovation Academy for Microsatellites of Chinese Academy of Sciences, Shanghai, China.

J. Yi is with the Department of Mechanical and Aerospace Engineering, Rutgers University, Piscataway, NJ 08854 USA (e-mail: jgyi@rutgers.edu).

T. Liu is with the the State Key Lab of Fluid Power and Mechatronic Systems and the School of Mechanical Engineering, Zhejiang University, Hangzhou, Zhejiang 310027, China (email: liutao@zju.edu.cn).

Digital Object Identifier: 10.1109/TASE.2019.2922068

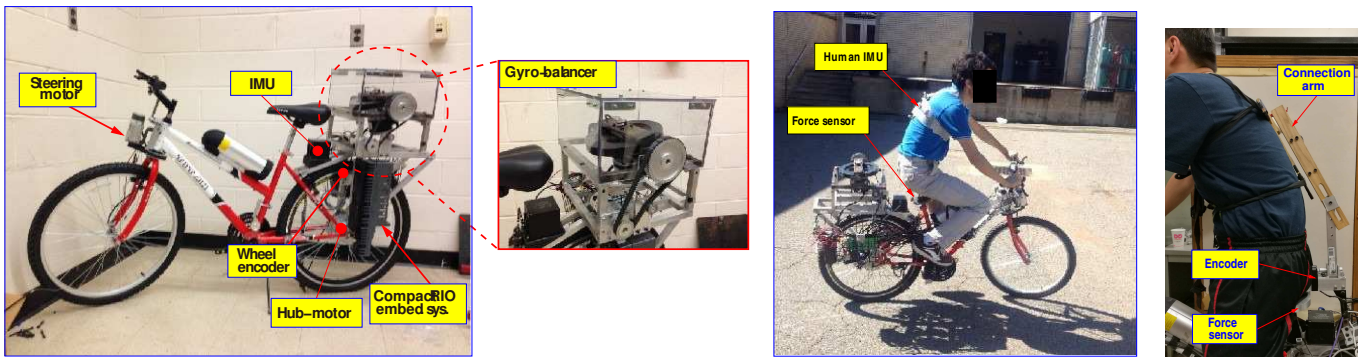

(a) (b) (c)

Fig. 1. (a) The Rutgers bikebot system. (b) Human riding experiment. (c) Upper-body pose estimation fixture.

(PD)-like feedback control law is proposed to describe the rider's steering mechanism for balance tasks. Such a neuro-musculoskeletal model is inspired by the work of stance balance strategy in [3], [6]. For validating and understanding these control models, extensive riding experiments are designed using the newly developed bikebot platform. With the above-mentioned models, the closed-loop dynamics of the rider-bicycle systems is obtained with four time delays. We take advantages of the recent advances in analysis tools for time-delay dynamical systems [24]–[28] and apply to the linearized dynamics around the equilibrium points. The quasi-polynomial mapping-based root-finder (QPMR) [29] is used to compute the right most roots of the closed-loop characteristic equation. The stability results are compared and validated with experiments.

Besides normal riding condition, we also conduct rider-bikebot riding experiments under three types of perturbations. The external torque perturbation is first introduced by the bikebot's gyro-balancer, the second type of the perturbation is the visual feedback blocking and distortion, and the last type of the perturbation is the steering actuation time delay. One of the motivations to introduce these perturbations in experiments is to excite the rider-bicycle interactions such that the human balance control model can be identified and estimated. The other goals include sensitivity analysis of the model parameters of the identified human sensorimotor balance models. We use the bicycle balance metric developed in [30] to quantify the human motor skills and performance.

The main contribution of the work are two-folds. First, the new sensorimotor models for human steering and body movements extend and complement the existing methods to capture human balance and control strategies. These human control models provide enabling tools to analyze human-in-the-loop dynamic systems. Second, the stability analysis of the rider-bicycle system is new and can be directly used for designing the bicycle-based rehabilitation devices. The perturbed human riding experiments provide a methodology to understand and estimate the sensitivity of the model parameters on human balance performance. The approaches are also potentially extendable to other types of physical human-machine/robot interactions. Comparing with the previously presented conference publication [31], this paper contains new analyses and results in several aspects. The human control models are significantly different with those in [31] to better capture the experiments and observations. Additional time delay constants are considered in the human control models and therefore, different stability analysis tool is used in this work. Moreover, the conducted experiments are completely new and different with these in [31]. We introduce multiple perturbations in experiments and consider the sensitivity analysis with different model parameters. The models, analyses and experiments bring new results that have never been published in previous conference papers, including [31].

The rest of the paper is organized as follows. The rider-bicycle dynamic model is presented in Section II. In Section III, the human balance control strategy is discussed and stability analysis is also included. Section IV describes the experiments and the methods. Experimental results are presented in Section V. Finally, we summarize the concluding remarks in Section VI.

II. Dynamic Models of Rider-Bicycle System

Fig. 1(a) shows the bikebot platform developed at Rutgers University [32]. Bikebot is a modified bicycle system with an additional gyro-balancer to create disturbing balance torques, and computer-controlled steering and pedaling actuation. Detailed description of the bikebot is presented in Section IV-A. Fig. 1(b) shows an example of human riding experiment on the bikebot. When human ride the bikebot, the handlebar angle is measured and the onboard embedded system regulates the actual steering angle to follow the handlebar angle profile. The bikebot speed is also controlled by the onboard computer system with a turning knob for the rider to manually adjust the reference velocity with a speed display. The main purpose to develop the bikebot is to provide a robotic platform to excite the human balance sensorimotor mechanisms.

Fig. 2 shows the schematic of the kinematic configuration of the rider-bikebot system. Two coordinate frames are used: an inertial frame $\mathcal{N} : XYZ$ and a body-fixed frame $\mathcal{B} : xyz$ with the origin C_2 is attached on the rear wheel contact point, the x-axis is along the wheelbase C_1C_2 and the z-axis points downward, the same as the Z-axis. Frame $\mathcal{B}$ is considered by rotating $\mathcal{N}$ by bikebot roll angle φ_b along the X-axis and yaw angle ψ around the Z-axis. The bikebot is modeled as a rigid

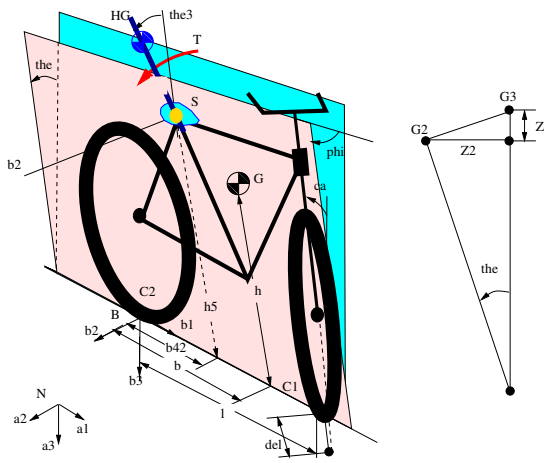

Fig. 2. Kinematic schematics of the rider-bicycle systems (left) and the vertical position changes of the center of mass of the bicycle/rider due to steering and rolling effects (right).

body with mass m_b and inertial moment J_b around the x-axis. The mass center G and the seat position are respectively located at $[l_b \ 0 \ -h_b]^T$ and $[l_s \ 0 \ -h_s]^T$ in $\mathcal{B}$. The bikebot wheelbase is denoted as l, the caster angle as ε, and the trail length as l_t. We also denote the steering angle as δ.

The rider's upper-body is considered as an inverted pendulum with its length denoted as h_h [33]. For simplicity, we only consider roll angle φ_h in the human coronal plane (i.e., relative to the bikebot frame in the x-z plane of $\mathcal{B}$). The bikebot orientation is captured by yaw angle ψ and roll angle φ_b. With the nonholonomic constraint at C_2, the bikebot velocity is denoted by v_r, namely, the longitudinal velocity of C_2. With the above configuration, the bikebot yaw rate is calculated as [34], [35]

$$\dot{\psi} = \frac{v_r \tan\delta \, \mathrm{c}_\varepsilon}{l \, \mathrm{c}_{\varphi_b}}, \tag{1}$$

where notations $\mathrm{c}_x := \cos x$ and $\mathrm{s}_x := \sin x$ are used for variable x in the above equation and throughout the rest of the paper. The yaw acceleration has the form as

$$\ddot{\psi} = \frac{\mathrm{c}_\varepsilon}{l \, \mathrm{c}^2_{\varphi_b}} \left(\dot{v}_r \, \mathrm{c}_{\varphi_b} \tan\delta + v_r \, \mathrm{s}_{\varphi_b} \, \dot{\varphi}_b \tan\delta + \frac{v_r \, \mathrm{c}_{\varphi_b} \, \dot{\delta}}{\mathrm{c}^2_\delta} \right). \tag{2}$$

From (2), under constant v_r and small φ_b, it is straightforward to obtain $\ddot{\psi} \approx \frac{v_r \dot{\delta} \, \mathrm{c}_\varepsilon}{l \, \mathrm{c}^2_\delta}$.

Because of the non-zero caster angle ε and trail length l_t, even for the same roll angle φ_b, the changes of the vertical height of the bicycle and rider mass centers are different with varying steering angle δ. As shown in Fig. 2, due to steering effect, the vertical position changes of points G and S, denoted respectively as Δz_G and Δz_S, are expressed as [34], [36]

$$\Delta z_G = \frac{l_b g l_t \, \mathrm{c}^2_\varepsilon}{l} \tan\delta \tan\varphi_b, \ \Delta z_S = \frac{l_s g l_t \, \mathrm{c}^2_\varepsilon}{l} \tan\delta \tan\varphi_b.$$

Therefore, the lateral movements of G/S due to Δz_G and Δz_S are obtained as $\Delta y_G = \Delta z_G / \tan\varphi_b$ and $\Delta y_S = \Delta z_S / \tan\varphi_b$, respectively. Similar to [37], the total gravitational balancing torque u_δ due to steering effect is calculated approximately as

$$u_\delta = -\left(m_b l_b + m_h l_s\right) \frac{g l_t \, \mathrm{c}^2_\varepsilon}{l} \tan\delta. \tag{3}$$

Therefore, the steering actuation generates a gravitational-related balancing torque that is independent with velocity v_r.

We use Lagrangian equations to obtain the motion dynamics for the rider-bikebot system. Denoting the generalized coordinate for the system as $\boldsymbol{q} = [\varphi_b \ \varphi_h]^T$, the equations of motion are obtained as [33], [38]

$$\boldsymbol{M}(\boldsymbol{q})\ddot{\boldsymbol{q}} + \boldsymbol{C}(\boldsymbol{q}, \dot{\boldsymbol{q}}) + \boldsymbol{G}(\boldsymbol{q}) = \boldsymbol{u}, \tag{4}$$

where matrices $\boldsymbol{M}(\boldsymbol{q})$, $\boldsymbol{C}(\boldsymbol{q}, \dot{\boldsymbol{q}})$ and $\boldsymbol{G}(\boldsymbol{q})$ are given in (5) on the top of this page. In (4), the input is defined as $\boldsymbol{u} = [0 \ u_h]^T$, where u_h represents the human trunk driving torque. Plugging (1) and its time derivative into (4), we obtain the motion equations of the rider-bikebot system with the rider applied torque u_h and the steering actions $u_s = \tan\delta$ and its derivative as control inputs.

III. Human Balance Control Models and Stability Analysis

A. Human Balance Control Models

1) Human body movement balance model: In [18], a human balance model is presented to capture the sensorimotor mechanisms to ride a stationary bicycle. Fig. 3 illustrates the block diagram of the human balance leaning control. The model captures the body intrinsic stiffness, short-, medium- and long-term phasic mechanisms due to proprioception, vestibular and visual sensory, respectively. For example, the intrinsic stiffness

$$\boldsymbol{M}(\boldsymbol{q}) = \begin{bmatrix} m_b h_b^2 + m_h \left(h_s^2 + h_h^2 + 2 h_s h_h \, \mathrm{c}_{\varphi_b}\right) + J_b & m_h \left(h_h^2 + 2 h_s h_h \, \mathrm{c}_{\varphi_b}\right) \\ m_h \left(h_h^2 + 2 h_s h_h \, \mathrm{c}_{\varphi_b}\right) & m_h h_h^2 + J_h \end{bmatrix}, \tag{5a}$$

$$\boldsymbol{C}(\boldsymbol{q}, \dot{\boldsymbol{q}}) = \begin{bmatrix} -\left(m_b h_b^2 \, \mathrm{s}_{\varphi_b} \mathrm{c}_{\varphi_b} + m_h h_h^2 \, \mathrm{s}_{\varphi_b + \varphi_h} \mathrm{c}_{\varphi_b + \varphi_h} + h_s h_h \, \mathrm{c}_{2\varphi_b + \varphi_h}\right) \dot{\psi}^2 + \left(m_b h_b l_b \, \mathrm{c}_{\varphi_b} + m_h h_s l_s \, \mathrm{c}_{\varphi_b} + \right. \\ \left. m_h h_h l_s \, \mathrm{c}_{\varphi_b + \varphi_h}\right) \ddot{\psi} + \left(m_b h_b \, \mathrm{c}_{\varphi_b} + m_h h_s \, \mathrm{c}_{\varphi_b} + m_h h_h \, \mathrm{c}_{\varphi_b + \varphi_h}\right) v_r \dot{\psi} + \left(m_b l_b \, \mathrm{c}_{\varphi_b} + m_h l_s \, \mathrm{c}_{\varphi_b}\right) g l_t \, \mathrm{c}_\varepsilon \, v_r^{-1} \dot{\psi} \\ -m_h h_h h_s \, \mathrm{s}_{\varphi_h} \, \dot{\varphi}_h \left(2\dot{\varphi}_b + \dot{\varphi}_h\right) \\ \hline m_h h_h h_s \, \mathrm{s}_{\varphi_h} \, \dot{\varphi}_h^2 - \left(m_h h_s h_h \, \mathrm{s}_{\varphi_b} \mathrm{c}_{\varphi_b + \varphi_h} + m_h h_h^2 \, \mathrm{s}_{\varphi_b + \varphi_h} \mathrm{c}_{\varphi_b + \varphi_h}\right) \dot{\psi}^2 + m_h h_h l_s \, \mathrm{c}_{\varphi_b + \varphi_h} \ddot{\psi} + \\ m_h h_h \, \mathrm{c}_{\varphi_b + \varphi_h} \, v_r \dot{\psi} \end{bmatrix}, \tag{5b}$$

$$\boldsymbol{G}(\boldsymbol{q}) = \begin{bmatrix} -m_b h_b g \, \mathrm{s}_{\varphi_b} - m_h h_s g \, \mathrm{s}_{\varphi_b} - m_h h_h g \, \mathrm{s}_{\varphi_b + \varphi_h} \\ -m_h h_h g \, \mathrm{s}_{\varphi_b + \varphi_h} \end{bmatrix}. \tag{5c}$$

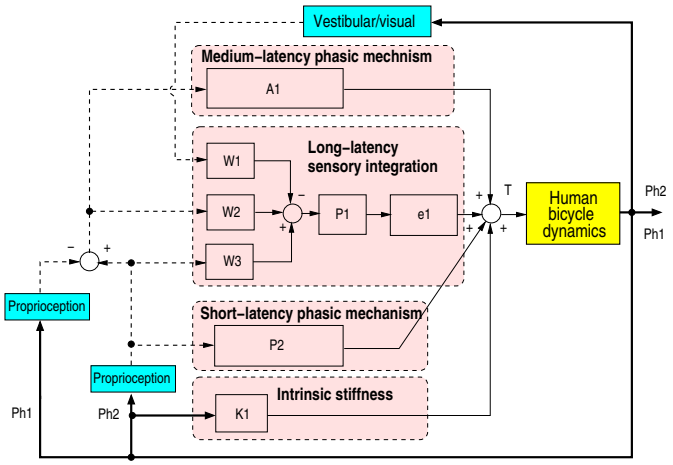

Fig. 3. A block diagram that represents the human motor control model for the body leaning torque $u_h(t)$ [18]. The block diagram mainly represents the relationship between sensory feedback of bicycle and rider upper-body roll angles (i.e., φ_b and φ_h) and human leaning torque $u_h(t)$.

mechanism provides a proportional torque (i.e., stiffness coefficient K_{in}) to the (relative) roll angle φ_h. The short-latency phasic mechanism (with coefficient B_{sl} and delay τ_{sl}) captures the upper-body tilting velocity $\dot{\varphi}_h$. The short-latency phasic mechanism is based on the proprioception sensory feedback. The medium-latency phasic mechanism (with delay τ_{ml} and coefficient B_v) generates a torque that is proportional to the upper-body angular velocity $\dot{\varphi}_h$. Finally, the long-latency sensory integration mechanism generates the torque through a neural proportional-integral-derivative (PID) controller with long latency τ_{ll}.

For the above discussion, we propose the following body leaning torque model

$$\begin{aligned} u_h(t) &= k_{h0}\varphi_h(t) + k_{h1}\varphi_b(t-\tau_1) + k_{h2}\dot{\varphi}_b(t-\tau_2) \\ &\quad + k_{h3}\varphi_h(t-\tau_1) + k_{h4}\dot{\varphi}_h(t-\tau_2), \end{aligned} \tag{6}$$

where k_{hi}, $i = 0, \cdots, 4$, are the control gains and $\tau_1, \tau_2 > 0$ are time-delay constants. The control model (6) is considered as a similar but simplified structure as shown in Fig. 3. The first term represents the passive torque proportional to $\varphi_h(t)$ with intrinsic stiffness k_{h0}. The rest four terms in (6) contain the time-delay of the bikebot roll angle φ_b and the upper-body roll angle φ_h and their derivatives. These terms are considered as a simplified representation of the short-, medium- and long-term phasic mechanisms due to proprioception, vestibular and visual sensory shown in Fig. 3. For example, the PD control structure with gains k_{h1} and k_{h3} for position and k_{h2} and k_{h4} for velocity are used to capture the resultant effects of coefficients B_{sl}, B_v, and the PID-gain in the model described in Fig. 3. The model (6) uses only two time delays τ_1 and τ_2 rather than three in [3], [18] to simplify the analysis. The model (6) is validated by the experimental results in Section IV.

Fig. 3 mainly represents the information and signal flow for the human leaning torque model and does not include human or bicycle dynamics. The rider-bicycle dynamics (4) are included in the "Human-bicycle dynamics" block in the figure. The main portion of Fig. 3 includes a three-delayed structure that represents phenomenological relationship between the human leaning control torque u_h and rider and bicycle angles (the angular rates are actually calculated through these derivative terms (as Laplace operator s) in the figure.)

2) Steering balance model: For human steering control, we propose a similar PD structure model as

$$\begin{aligned} \delta(t) &= \frac{1}{v_r^2}\Big[k_{b1}\varphi_b(t-\tau_3) + k_{b2}\dot{\varphi}_b(t-\tau_4) \\ &\quad + k_{b3}\varphi_h(t-\tau_3) + k_{b4}\dot{\varphi}_h(t-\tau_4)\Big], \end{aligned} \tag{7}$$

where τ_3 and τ_4 are the time delays constants and k_{bi}, $i = 0, \cdots, 4$, are the constant control gains. Given the double inverted-pendulum model, the human controlled steering angle is related to both the bikebot and the upper-body roll angles. For the upright equilibria, that is, $\varphi_{be}(t) = \varphi_{he}(t) = 0$, each term in (7) is indeed the errors $\varphi_b - \varphi_{be}$ or $\varphi_h - \varphi_{he}$ and their derivatives with the time delays. Similar to the model (6), the PD feedback structure is used. Similar to (6) and for simplicity, the time delays in the bikebot and upper-body roll angles terms are the same and also the same time delay for the roll angular velocities. For (4), one dominating term is the centrifugal torque that is proportional to $v_r\dot{\psi}$. Given (1), the centrifugal torque is proportional to v_r^2 and therefore, the steering model in (7) contains the factor v_r^{-2}. Moreover, we also observe in experiments that with faster moving speed v_r, the steering control is less aggressive and this matches the mathematical relationship in (7). We will also show the experimental validation of (7) in Section IV.

The leaning torque control given in (6) is a phenomenological model and does not explicitly include terms that represent physical rider-bicycle interactions dynamics, such as centrifugal or gravitational forces, etc. The model can however be interpreted to include these dynamic effects implicitly. For instance, the gravitational force is related to roll angles and is indeed proportional to a linear combination of bicycle roll angle $\varphi_b(t)$ and upper-body roll angle $\varphi_h(t)$. Therefore, its effect has been captured by the first two terms of the right-side of (6). For centrifugal force, its magnitude is proportional to $v_r\dot{\psi}$. In experiments, velocity variation is not large and by (1), yaw rate $\dot{\psi}$ is directly related to steering angle δ. The influence of the centrifugal force on $u_h(t)$ is then related to δ and from (7), it is again a function of velocity v_r and combination of roll angles and angular rates. Therefore, model (6) implicitly includes the dynamic effects. Moreover, similar forms in (6) and (7) are taken and this treatment would also help stability analysis. Indeed, the experiments in Section IV demonstrate that these models capture rider performance.

It is also noted that unlike the internal model [39] that incorporates both feedback and feedforward mechanism, the human control models (6) and (7) only include feedback terms. We do not use internal model in this study primarily for several considerations. First, the internal model has been mainly used to capture simple human movement mechanism such as arm reaching motion (e.g., [40]). It is not clear whether the internal model can be applied to the complex motor skills such as bicycle balance. Second, the focus of

this paper lies in experienced rider balance behavior and stability analysis. It is out of scope of this paper to find out how the bicycle riding training can improve riders' balance capability and performance. Therefore, the commonly used feedforward mechanism in internal model applications is not included in the human control models. Nevertheless, it is of interest to incorporate the internal model concept and bring the feedforward mechanism into the human control model as one of future research directions.

Remark 1: Comparing with the model in [20] with five model parameters for both platform balancing and path-following tasks, the proposed models (6) and (7) provide additional important features. The proposed models explicitly capture the body leaning motion, which is important for the platform balancing task. The models also explicitly consider the sensorimotor time delays. The existence of time delays in human sensorimotor are observed in various balancing systems [1]–[6] and we shall include these delays in bicycle riding task. The rider control models enable the stability analysis of the closed-loop systems. We also conduct the sensitivity study of the model parameters under various sensory feedback perturbations. These are complementary to the results in [20].

Remark 2: We focus on the platform balancing task in this paper and the rider control models are proposed by this consideration. Although they are not extensively validated by experiments, the rider control models in this paper might be possibly modified for path-following task [15]. Indeed, in [30] we presented a nonlinear control design (i.e., external/internal convertible (EIC)-based control) for an autonomous bicycle for path-following task. The rider steering angle output profiles are similar to the EIC-based controller outputs. Extensive validation of the rider control models for path-following performance is out of the scope of this paper.

Remark 3: The steering control model (7) uses the steering angle, rather than steering torque, as its output for several considerations. Bicycles have relatively light steering components, a small cast angle and small tire-road contact forces, and all of these conditions result in the fast steering dynamics from the rider steering torque input to the steering angle output. From balance viewpoint, the bicycle's self-stabilizing property in [12], [14] is obtained by considering the steering torque as the control input. However, this treatment is primarily for *riderless* or *handlebar-free steering* cases, while in our study, the riders always put their hands on the steering handlebar and also regulate the controlled steering actuation. With the rider's balance actuation, the steering angle is considered as the controlled input to the rider-bicycle systems. Moreover, the experimental results in Section IV and in [30] confirm that the steering angle design produced satisfactory balance performance. Besides our work, other control design and experiments such as those in [15], [37] also neglect the steering dynamics and use the steering angle (rather than the steering torque) as the input to obtain satisfactory results. Finally, inclusion of the steering dynamics would increase the complexity of the closed-loop stability analysis and might even prevent from obtaining the stability and parameter sensitivity results, which is one of the main goals of this paper.

B. Rider-Bicycle System Stability

Since dynamic model (4) is nonlinear and the human balance models (6) and (7) contain time-delay terms, the stability analysis is conducted by using the linearized dynamics with time delays. The equilibria of the system states are zeros and the linearized dynamics approximately capture the nonlinear stability properties [17], [18]. After plugging (6) and (7) into (4), the linearized dynamic models around the equilibria are

$$\ddot{\boldsymbol{q}}+\boldsymbol{T}_2\ddot{\boldsymbol{q}}(t-\tau_4)+\sum_{i=1}^{4}\left[\boldsymbol{B}_i\dot{\boldsymbol{q}}(t-\tau_i)+\boldsymbol{K}_i\boldsymbol{q}(t-\tau_i)\right]+\boldsymbol{K}_0\boldsymbol{q}=\boldsymbol{0}, \tag{8}$$

where gain matrix $\boldsymbol{T}_2 \in \mathbb{R}^{2\times 2}$ is introduced by the derivative terms in the steering model, $\boldsymbol{B}_i, \boldsymbol{K}_i \in \mathbb{R}^{2\times 2}$, $i = 0, \cdots, 4$, are the damping and stiffness matrices, respectively. We do not list the detailed, lengthy formulation for these matrices.

Defining $\boldsymbol{x} = [\boldsymbol{q} \;\; \dot{\boldsymbol{q}}]^T \in \mathbb{R}^{4\times 4}$, the closed-loop system dynamics (8) becomes

$$\dot{\boldsymbol{x}} + \boldsymbol{D}_2\dot{\boldsymbol{x}}(t-\tau_4) + \boldsymbol{A}_0\boldsymbol{x} + \sum_{i=1}^{4}\boldsymbol{A}_i\boldsymbol{x}(t-\tau_i) = \boldsymbol{0}, \tag{9}$$

where

$$\boldsymbol{D}_2 = \begin{bmatrix}\boldsymbol{0}_2 & \boldsymbol{0}_2\\ \boldsymbol{0}_2 & \boldsymbol{T}_2^T\end{bmatrix},\ \boldsymbol{A}_0 = \begin{bmatrix}\boldsymbol{0}_2 & -\boldsymbol{I}_2\\ \boldsymbol{K}_0^T & \boldsymbol{0}_2\end{bmatrix},\ \boldsymbol{A}_i = \begin{bmatrix}\boldsymbol{0}_2 & \boldsymbol{0}_2\\ \boldsymbol{K}_i^T & \boldsymbol{B}_i^T\end{bmatrix}$$

for $i = 1, \cdots, 4$, and $\boldsymbol{I}_n$ and $\boldsymbol{0}_n$ are the $n \times n$ identity and zero matrices, respectively. Taking the Laplace transformation, the characteristic equation of (9) is obtained as

$$\det\left[\left(\boldsymbol{I}_4 + \boldsymbol{D}_2 e^{-\tau_4 s}\right)s + \boldsymbol{A}_0 + \sum_{i=1}^{4}\boldsymbol{A}_i e^{-\tau_i s}\right] = 0, \tag{10}$$

where the time delays are introduced in the exponential terms. For presentation convenience, we denote the right-most root of (10) as λ_0 and we will use λ_0 to determine the time-delay system stability. If the value of the real part of λ_0 is negative, that is, $\mathrm{Re}(\lambda_0) < 0$, the closed-loop system is stable. A system with smaller real part values $\mathrm{Re}(\lambda_0)$ is considered to be more robustly stable. A quasi-polynomial mapping-based root finder [41] is used to compute the stability region given by (10). We will also use values of $\mathrm{Re}(\lambda_0)$ as an index to illustrate the stability property in later sections.

IV. Experiments

A. Bikebot System

The bikebot system is shown in Fig. 1(a). The platform is modified from a mountain bicycle with added onboard sensors and actuators. A real-time embedded system (cRIO model 9082 from National Instruments Inc.) is used to collect the sensor measurements and also for motion control at a frequency of 100 Hz. The bikebot velocity v_r is measured by the encoder mounted on the rear wheel, and the steering angle δ and the handlebar rotating angle are measured respectively by two encoders on the steering structure. The rider's leaning angle φ_h is obtained by a rolling arm and an encoder that is rigidly connected to the upper-body segment; see Fig. 1(c). The bikebot roll angle φ_b and yaw angle ψ are obtained by

(a) (b)

Fig. 4. (a) Handlebar and front wheel steering angle sensors and front wheel steering actuator. (b) Visual blocking glasses and mirror glasses.

a high-accuracy inertial measurement unit (IMU) (model 801 from Motion Sense Inc.) mounted on the frame.

The bikebot motion is powered by a hub motor while a human rider can still manually pedal. The front wheel frame might be connected or disconnected to the handlebar by a mechanical switch. When connected, the steering action is operated by the rider, like a normal bicycle; while disconnected, the steering actuation is driven by a DC motor (with an integrated encoder); see Fig. 4(a). In this case, the human rider can still turn the handlebar and the turning angle is obtained by the encoder. The onboard steering controller is designed to follow the human steering, or a modified steering action. For example, the controlled steering angle is designed to follow the rider's input with a time delay. To further perturb the rider, we designed and installed a gyro-balancer on the rear rack; see Fig. 1(a). The gyro-balancer provides a rolling torque that is generated by the gyroscopic motion of a high-speed spinning flywheel (around 1000 rpm) with a controlled pivoting rotation. By using the steering actuator and the gyro-balancer, the bikebot system creates perturbations to which the human rider needs to react for balance keeping. By measuring the rider's reactions, we identify the human balance control behaviors and therefore estimate the human balance model parameters.

B. Riding Experiments

Five subjects (all males with ages: 29.8 ± 3.4, heights 1.73 ± 0.05 m, and weights 66.8 ± 7.5 kg) were recruited for the experiments. All of the participants were chosen from students at Rutgers University and were reported to be in a good health condition. All subjects were reported by themselves to have at least five years' bicycle riding history and were considered as experienced riders. An informed consent form was signed by all subjects and the testing protocol was approved by the Institutional Review Board (IRB) at Rutgers University.

In all tests, the subjects were required to ride the bikebot only for keeping balance on an open parking field. The bikebot was controlled at a constant speed (ranging from 1.7-2.3 m/s and speed variation is less than 0.2 m/s in each test). Three types of perturbations were used separately in these tests: the external balancing torque perturbation, the visual perturbation and the steering actuation time-delay perturbation. The riding experiments were conducted by three groups, following the above-mentioned three types of perturbations. The first group was the normal riding with perturbed rolling torques by the gyro-balancer. The subjects were informed the possible rolling perturbation but they did not know when the perturbation was applied. The generated perturbation was an impulse torque by suddenly pivoting of the spinning flywheel. In the second group of experiments, the riders were visually perturbed as well as the external torque perturbations by the gyro-balancer. To generate the visual perturbations, two types of eye glasses were wore by the riders separately. Fig. 4(b) shows these two types of eye glasses. The viewed images of the first pair of glasses (called Glasses I as shown on the top of Fig. 4(b)) were partially blocked by translucent tapes. The subjects cannot see the environment objects completely and the sensing images were blocked partially. The images of the second pair of glasses (called Glasses II as shown on the bottom of Fig. 4(b)) were distorted by a set of internal mirrors. When they wore Glasses II, the subjects felt dizzy with the distorted images and it took a few hours to get used to it. It is generally considered that Glasses II generate much more visual and perception distortion and perturbation than these of Glasses I.

The third set of experiments were conducted with time-delay perturbations in steering actuation. In these tests, the handlebar and the front wheel frame were mechanically disconnected. The rider rotated the handlebar and the actual steering angle was controlled by the steering motor to track the human input angle with a designed time delay. The goal of this set of experiments is to understand how the steering perturbation and delay affect the riding performance and stability. The time-delay was set initially from 80 ms with an incremental 50 ms delay in each experiment until the subjects cannot maintain balancing properly. These time-delay values are chosen using the same range of the human neuro-controller delays in [3].

We label five subjects as A to E. Before riding data was collected, each subject was asked to ride the bikebot for about 15 to 30 mins. Under each experimental condition, the subject was asked to repeat the tests two or three times and all experimental data were recorded and processed. All subjects completed the first group of normal riding experiments and the second group of visual perturbations experiments with wearing Glasses I. However, subject E cannot ride the bikebot while wearing Glasses II. For the third group of riding experiments, subject A can ride and keep balance at time delays 80, 130, 180, and 230 ms, subjects B and C finished successfully with 80, 130, and 180 ms, and subjects D and E can only ride successfully at 80 and 130 ms.

C. Riding Performance Metrics

We use the value of $\mathrm{Re}(\lambda_0)$ of (10) as an indicator to quantify the system stability. To quantify the riding balance skills, we use the balance equilibrium manifold (BEM) concept that was introduced in [30] as a performance metric. The basic idea of the BEM is to calculate the balanced bicycle and rider upper-body roll angles under the human control.

We use the first dynamics equation in (4) to define the BEM. For given rider steering and pedaling inputs, we compute the required balance torque by the body movements and these torques due to the bicycle roll motion. From the first equation of (4), if the difference of the calculated required torque and rider-bicycle rolling torque is zero, the bicycle roll angle φ_b and the rider upper-body roll angle φ_h maintain at their equilibria. The calculation of $F(\boldsymbol{q}, \delta, \dot{\delta})$ in (11) on the top of this page captures the net balancing torque for the rider body movement under the equilibrium conditions. The smaller value of $|F(\boldsymbol{q}, \delta, \dot{\delta})|$, the closer of the roll angles to their equilibria. Considering $F(\boldsymbol{q}, \delta, \dot{\delta})$ over a time interval $[t_1,\, t_2]$, we use the following balance metric (BM) index as

$$BM = \frac{1}{t_2 - t_1} \int_{t_1}^{t_2} |F(\boldsymbol{q}, \delta, \dot{\delta})| dt. \tag{12}$$

A smaller BM value implies closer to the balance equilibria and therefore, more graceful and skillful in bikebot riding.

V. Results

A. Model Validation Results

To validate the rider-bikebot model (4), we take an inverse dynamics approach to calculate and compare the resultant torques by the model using the kinematics measurements. The inverse dynamics (rather than forward dynamics) validation is used primarily because in forward dynamics calculation, integration of the differential equation of the unstable rider-bicycle dynamic system might be sensitive to slightly imprecise values of the model parameters. Fig. 5 shows the experimental validation results. In the figure, we plot the comparison values of the gravitational and the other terms in both equations of (4). Rather than comparing the sums of all the terms in (4) with zero, we here separately consider the gravitational-related torque and compare them with the sums of the rest terms because the former is relatively large and therefore, it is more effective to use this comparison for model validation. Fig. 5(a) shows the comparison of the first equation and Fig. 5(b) for the second equation of (4). The experimental data in these figures are taken from subject A and the human torque data u_h are calculated from the (seat) force sensor measurements [33]. It is clear from these figures that the dynamic model (4) captures the motion and interactions between the rider and the bikebot.

To identify the human steering and body movement models (6) and (7), we use the collected sensor data in each riding experiment run and then a least square method was used to fit the data. The time delay parameters do not appear as the linear terms in the model and therefore, it is difficult to use the least square method to estimate and obtain their values. We first treat and fix these time delays values in their feasible ranges. For example, time delay τ_{s1} is estimated to be in the range of $[0, 500]$ ms and we then search time delay τ_{s1} at $\tau_{s1} = k\Delta T$ s, $k = 0, \cdots, 50$, $k \in \mathbb{N}$, and ΔT is the sampling period (in the experiments $\Delta T = 10$ ms). We extend such searching for other time delays. With a fixed time delay in each search iteration, the least square method is then used to estimate the values of the control gains. For each set of estimated time delays and control gains, we compute the fitting errors. Finally, the set of the parameters that gives the smallest fitting error is chosen as the estimates of the control model parameters.

Fig. 6 shows the validation results in one experiment test by subject A. The model parameters were obtained by using the data collected in other experimental runs. The rider operated the bikebot in a straight-line-like trajectory and the bikebot roll angle was within 0.1 rad; see Fig. 6(a). The model predictions of steering angle δ and body leaning torque u_h match the sensor measurements in experiments, as shown in Fig. 6(b). These results confirm the human steering and body movement models. We estimate the model parameters in (6) and (7) for each subject. The parameter values are listed in Table I for the gains and Table II for the time delays. In the tables, we include the mean values and standard deviations of each model parameter and time delay. From the magnitudes of these parameters in the tables, we find that for the model (6), the values of passive stiffness parameter k_{h0} are slightly smaller than these of active controlled k_{h3}. Values of both k_{h0} and k_{h3} are much larger than these of gains k_{h1}, k_{h2} or k_{h4}. Therefore, the rider leaning torque is much more sensitive for the upper-body roll angle than that of the bikebot. Similarly, values of k_{b1} are much larger than these of gains k_{b2}, k_{b3} or k_{b4}. We also notice that the steering angle is sensitive to bikebot roll angle than that of rider upper-body roll angle. For The time delays of the steering control have overall much larger values than these of the body leaning control, similar to the previously reported results [42] in which the former and latter delays are around 200 and 100 ms, respectively.

The estimated values of the model parameters in Table I and plots in Fig. 6 are directly based on experimental data without using any low-pass filters. We calculate derivatives of roll angles in human control models (6) and (7) numerically and the calculations do not result in large numerical noises. This is probably due to several reasons. The bicycle roll angle φ_b and angular rate $\dot{\varphi}_b$ measurements are directly from IMU and output signals are already pre-processed and therefore smooth, as shown in Fig. 6(a). Another reason for no significant numeric errors is that the magnitudes of gains values for derivative terms in the control model are significant smaller than those of the proportional terms, as we mentioned above.

B. Control Models Parameters Analysis

The visual perturbations affect the human riding motor behaviors. Out of all control model gains, bikebot roll angle gain

$$\begin{aligned} F(\boldsymbol{q}, \delta, \dot{\delta}) \;=\; & -\Big[m_b h_b^2 \,\mathrm{s}_{\varphi_b}\,\mathrm{c}_{\varphi_b} + m_h\big(h_h^2\,\mathrm{s}_{\varphi_b+\varphi_h}\,\mathrm{c}_{\varphi_b+\varphi_h} + h_s h_h\,\mathrm{c}_{2\varphi_b+\varphi_h}\big)\Big]\dot{\psi}^2 + (m_b h_b l_b\,\mathrm{c}_{\varphi_b} + m_h h_s l_s\,\mathrm{c}_{\varphi_b} + m_h h_h l_s\,\mathrm{c}_{\varphi_b+\varphi_h})\ddot{\psi} \\ & + (m_b h_b\,\mathrm{c}_{\varphi_b} + m_h h_s\,\mathrm{c}_{\varphi_b} + m_h h_h\,\mathrm{c}_{\varphi_b+\varphi_h}) v_r \dot{\psi} - (m_b h_b\,\mathrm{s}_{\varphi_b} + m_h h_s\,\mathrm{s}_{\varphi_b} + m_h h_h\,\mathrm{s}_{\varphi_b+\varphi_h}) g - u_\delta. \end{aligned} \tag{11}$$

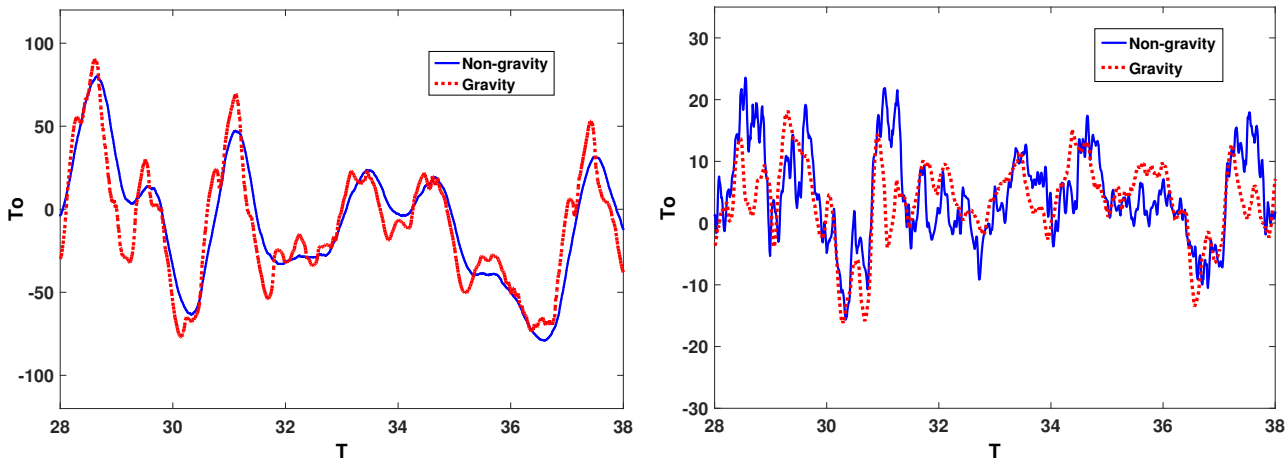

Fig. 5. Experimental results for rider-bikebot dynamics models validation. (a) Balancing torques in the first equation of (4). (b) Balancing torques in the second equation of (4).

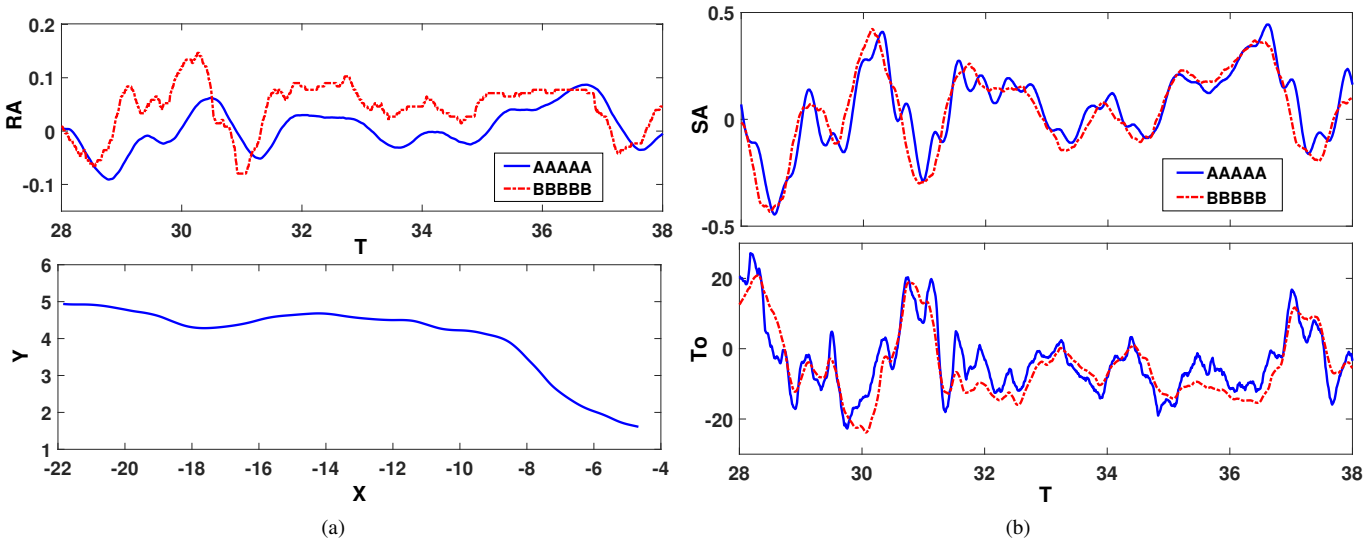

Fig. 6. Rider steering and body movement model validation results. (a) Rider upper-body and bikebot roll angle profiles (top plot) and bikebot position trajectory (bottom plot). (b) Validation results for the rider steering control model δ in (7) (top plot) and the body movement torque model u_h in (6) (bottom plot).

TABLE I
THE MEAN AND STANDARD DEVIATION OF THE HUMAN STEERING AND BODY MOVEMENT MODEL PARAMETERS.

Subject	k_{h0} (Nm/rad)	k_{h1} (Nm/rad)	k_{h2} (Nms/rad)	k_{h3} (Nm/rad)	k_{h4} (Nms/rad)	k_{b1} (m^2/s^2)	k_{b2} (m^2/s)	k_{b3} (m^2/s^2)	k_{b4} (m^2/s)
A	-96.3 ± 6.03	-66.2 ± 8.37	-8.23 ± 0.85	-139 ± 6.55	-19.6 ± 0.75	10.15 ± 0.54	1.24 ± 0.851	0.90 ± 0.20	0.92 ± 0.36
B	-97.7 ± 7.50	-71.5 ± 8.03	-7.13 ± 6.03	-135 ± 3.51	-13.0 ± 2.27	10.53 ± 0.51	1.13 ± 0.067	0.83 ± 0.06	1.18 ± 0.13
C	-99.5 ± 12.0	-74.6 ± 9.88	-10.3 ± 1.56	-111 ± 22.6	-17.7 ± 5.87	9.13 ± 0.28	1.62 ± 0.269	1.33 ± 0.42	1.01 ± 0.25
D	-81.0 ± 3.82	-84.0 ± 8.78	-4.2 ± 1.84	-85.0 ± 5.66	-11.7 ± 2.40	10.06 ± 0.15	1.07 ± 0.028	0.79 ± 0.23	1.00 ± 0.28
E	-80.0 ± 3.54	-81.9 ± 5.51	-9.0 ± 0.95	-75.7 ± 4.96	-16.9 ± 1.31	10.10 ± 0.64	1.605 ± 0.478	1.30 ± 0.28	1.18 ± 0.32

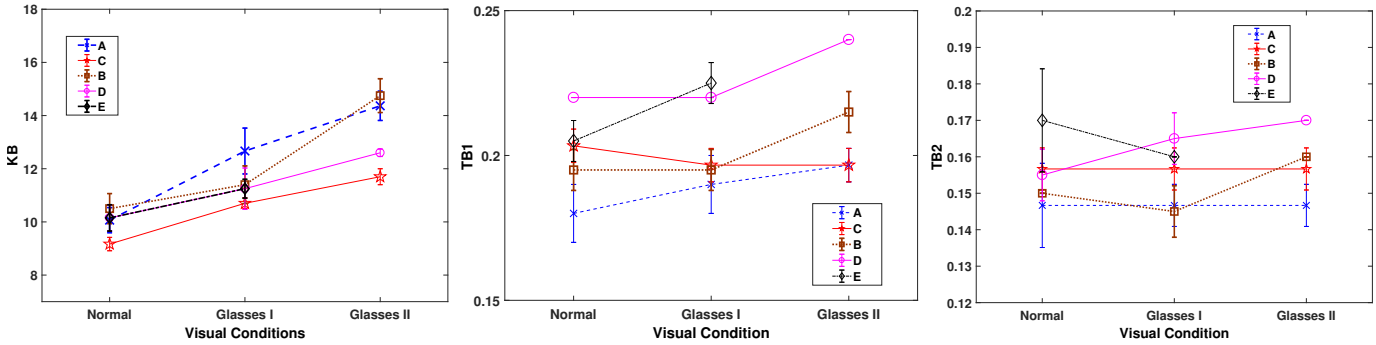

(a) (b) (c)

Fig. 7. Model parameter and time delay variations in experiments with five subjects under different visual conditions. (a) Parameter k_{b1}. (c) Time delay τ_3. (c) Time delay τ_4.

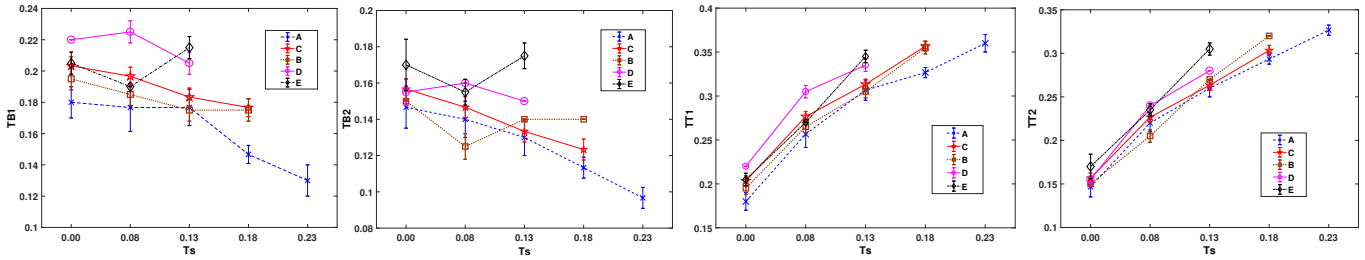

(a) (b) (c) (d)

Fig. 8. Human steering time delays under varying steering actuation delay τ_s. (a) Human steering control delay τ_3. (b) Human steering control delay τ_4. (c) Total steering delay τ_{s3}. (d) Total steering delay τ_{s4}.

TABLE II
IDENTIFIED HUMAN BODY MOVEMENT AND STEERING CONTROL TIME DELAYS.

Subject	τ_1 (ms)	τ_2 (ms)	τ_3 (ms)	τ_4 (ms)
A	163 ± 6	53 ± 12	200 ± 15	160 ± 11
B	147 ± 12	47 ± 12	190 ± 18	150 ± 13
C	140 ± 0	45 ± 7	190 ± 17	140 ± 17
D	145 ± 7	40 ± 0	170 ± 16	120 ± 12
E	135 ± 14	45 ± 7	130 ± 10	100 ± 6

k_{b1} has the most significant variation under visual perturbation. Fig. 7(a) shows the value change of k_{b1} under normal riding and riding with wearing Glasses I and II respectively for five subjects. It is clearly shown in these plots that after blocking the visual feedback, the values of gain k_{b1} increase about 0.5-2 consistently for each subject. Moreover, when the subjects wear Glasses II, the values of k_{b1} increase further about additional 0.5-2 for four out of five subjects (fifth subject E cannot ride stably.) Figs. 7(b) and 7(c) further show the values of time delays τ_3 and τ_4 under visual perturbations.

For the last group of experiments with delayed steering actuation, we denote the steering actuation time delay as τ_s. With human control delays τ_3 and τ_4 in (7), the total steering time delays are defined as

$$\tau_{s3} = \tau_3 + \tau_s,\ \tau_{s4} = \tau_4 + \tau_s.$$

Under varying τ_s (i.e., τ_{s3} and τ_{s4}), we have observed the changing values of steering control gain k_{b1} and leaning control gain k_{h1}, and time delays τ_3 and τ_4. These observations are illustrated in Fig. 8. We particularly choose to show these parameters because their changes are among the most significant. It is interesting to observe the decreasing trends of time delays τ_3 and τ_4 shown in Figs. 8(a) and 8(b), respectively. A large value of τ_s implies an increased difficulty of riding bikebot. Only subject A can control the bikebot at $\tau_s = 230$ ms. Subjects B and C can still ride the bikebot up to $\tau_s = 180$ ms and D and E at $\tau_s = 130$ ms. Although all subjects have different handling capabilities, it is interesting to notice in Figs. 8(c) and 8(d) that the maximum total time delays τ_{s3} and τ_{s4} of all subjects are about the same, that is, around 350 ms and 400 ms, respectively. These limits are probably the longest steering delays that experienced riders can handle.

To analyze the trend among all subjects, Fig. 9 shows the mean values and standard deviations of the above-mentioned parameters under varying τ_s and visual conditions. We clearly see a decreasing trend for gains k_{b1}, k_{h1}, and time delays τ_3 and τ_4 with increasing τ_s as shown in the top three plots in the figure. This implies that the riders enforce the dominating steering gain slightly by noticing the total time delays. The absolute values of the human control gain k_{h1} instead show an increasing trend with τ_s. Comparing with the values in normal riding case, the values of $|k_{h1}|$ at $\tau_s = 230$ ms increase about 20%. It seems that with an increased τ_s, the riders tried to use their body movements aggressively to keep balancing the platform. Under increasing severity of the visual conditions, the values of gain k_{b1} also increase as shown in the bottom plot

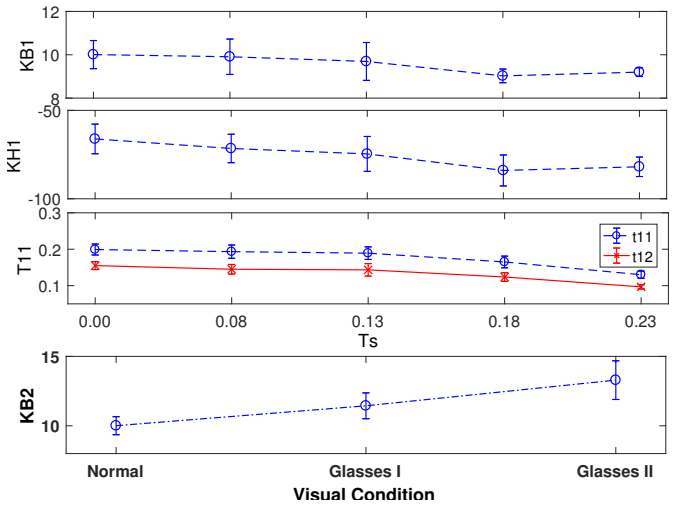

Fig. 9. Mean values and standard deviations across all subjects with respect to experiments conditions.

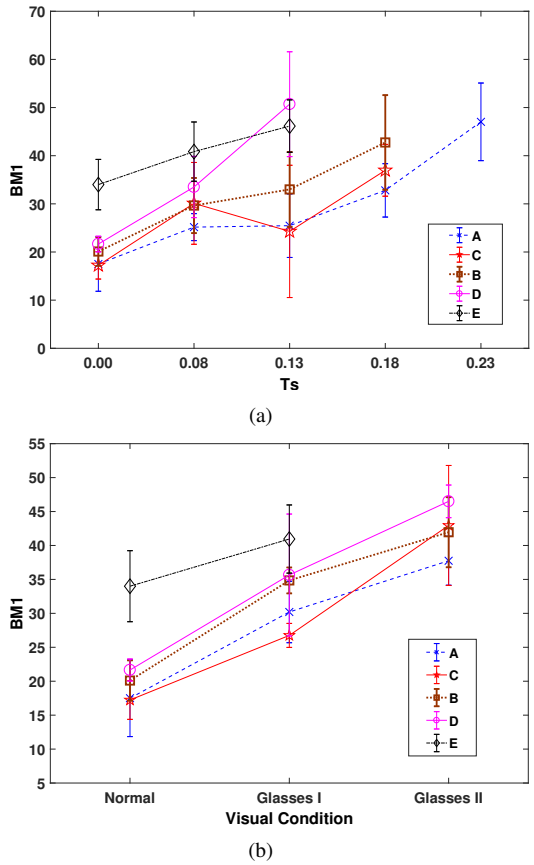

Fig. 10. Balance metric BM (mean and standard deviation) for five subjects under (a) varying steering actuation delay t_s and (b) visual conditions.

in Fig. 9. Gain k_{b1} and delay τ_4 show significantly changes under visual perturbation and increasing τ_s, respectively.

We calculate the balance metric BM under different riding conditions and Fig. 10 shows its mean and standard deviation values. Fig. 10(a) shows BM calculations for all subjects with increasing τ_s. The values of BM clearly increase with τ_s. The BM values are around 20 Nm for most riders (except subject E) at normal riding condition, i.e., $\tau_s = 0$. When $\tau_s = 230$ ms, the BM values increase to around 30-60 Nm. Similarly, the BM values also reach to around 35-50 Nm when the subject wears Glasses II as shown in Fig. 10(b). The deteriorated balance performance, that is, increased BM values, under varying riding conditions (either large delay or severe visual distortion) match the riding difficulty reported by the subjects.

C. Stability Results

From experiment observations, time delays τ_{s3} and τ_{s4} are critical to system stability. First, we choose gains k_{b1} and k_{b2} of (7) as an example to illustrate the stability analysis. Fig. 11 shows the stable region in the k_{b1}-k_{b2} plane under delay $\tau_{s3} = 200, 300$ and 350 ms. The stable region is defined as $\mathrm{Re}(\lambda_0) < 0$ for the roots of (10) under varying k_{b1} and k_{b2}. The values of all other model parameters and delays are listed in Tables I and II. Note that by Fig. 8(c), the range of $\tau_{s3} \in [200, 350]$ ms corresponds to steering delay $\tau_s \in [0, 230]$ ms. Besides the plotted regions (as solid red lines) by using the mean values of all model parameters and delays, we also include the stable regions using the sets of the model parameters one standard deviation smaller (green dot lines) and larger (blue dash lines) than the mean values.

By comparing these figures, we clearly observe that: (1) with increasing τ_s, the stable region becomes smaller as shown from $\tau_s = 0$ (i.e., $\tau_{s3} = 200$ ms) in Fig. 11(a) to $\tau_s = 230$ (i.e., $\tau_{s3} = 350$ ms) in Fig. 11(c). This is reasonable since it is more difficult for a rider to balance a bikebot with a long steering delay than that with a short delay; (2) It is interesting to see the identified (k_{b1}, k_{b2}) locations for each individual subject are related to the boundaries of the stable regions in the figure: with increasing delays, the subjects' balance performance became deteriorated and in the case of $\tau_s = 230$ ms in Fig. 11(c), all subjects performed closely around the stable region boundary. This is not surprising since as shown in Fig. 8(c), $\tau_{s3} = 350$ ms ($\tau_s = 230$ ms) is the maximum total (actuation) delay that all subjects can barely handle without loss of balance in riding experiments.

Similar to Fig. 11 to show the stable regions under different values of the control gains, Fig. 12 illustrates the stable region in the τ_{s3}-τ_{s4} plane along with all the subject time delays. The plots are split into three groups according to the three τ_{s3} intervals between 160 and 400 ms that are observed in experiments. The figures give an estimation of the ranges of the time delays τ_{s3} and τ_{s4} for system stability and also the observed subjects time delays. We also see that for almost all experiments, the subject time delays are located within but close to the stable region boundaries.

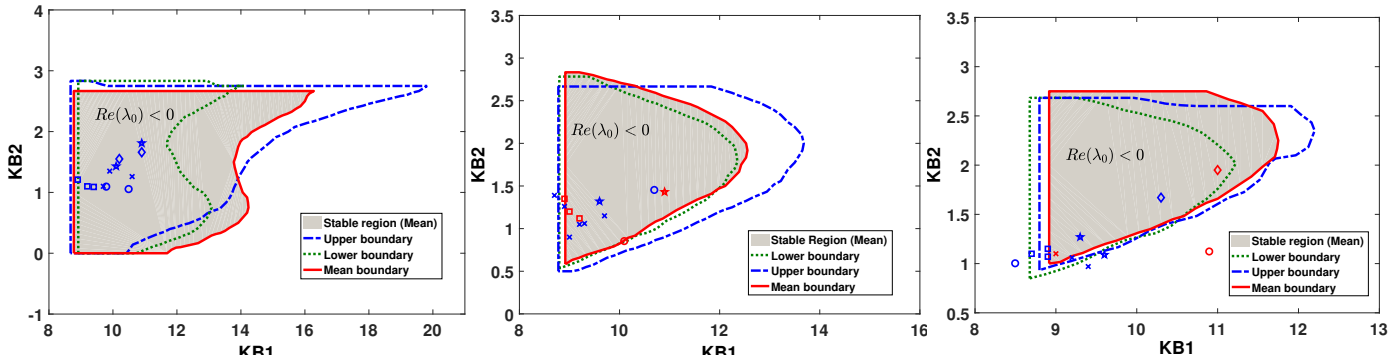

(a) (b) (c)

Fig. 11. Stable region in the k_{b1}-k_{b2} plane at different steering actuation delays. (a) $\tau_{s3} = 200$ ms. (b) $\tau_{s3} = 300$ ms. (c) $\tau_{s3} = 350$ ms. Red solid curve indicates the stable region calculated by the mean values of the control model parameters, green dot and blue dash curves indicate the stable regions calculated by the one standard deviation below and above the mean values of all model parameters, respectively. In the figures, individual dot represents each subject experiment test. "×", "□","⋆", "○" and "◇" marks indicate subjects A to E, respectively. Blue and red marks indicate the stable and unstable parameters point respectively. Note that the shaded areas are obtained by using the mean values of the control model parameters and for a particular subject, the stability is determined by using the control model parameters of that subject. Therefore, it is possible that red marks are located inside the shared areas.

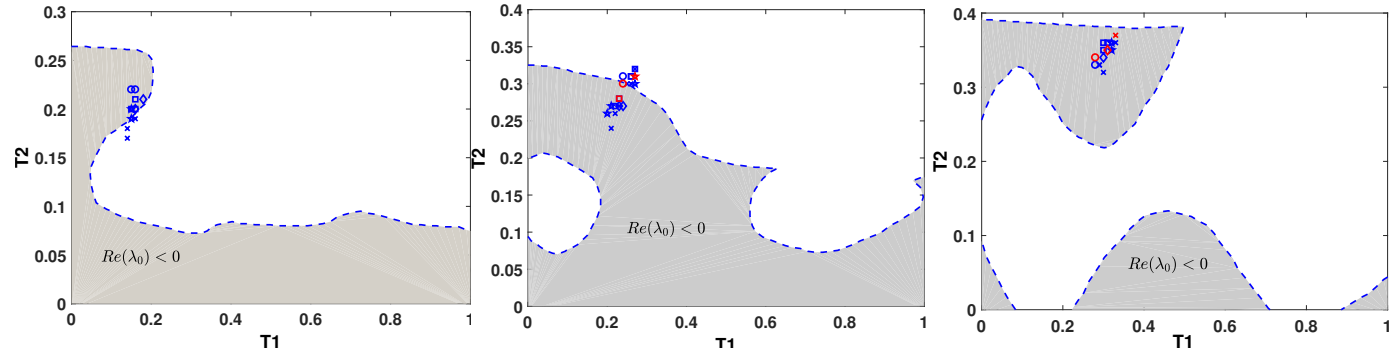

(a) (b) (c)

Fig. 12. Stable region in the τ_{s4}-τ_{s3} plane at different steering actuation delays. The stable regions are calculated using the experimental trials that are grouped by three different actuation delay intervals of τ_{s3}. (a) $\tau_{s3} \in [160, 240)$ ms. (b) $\tau_{s3} \in [240, 320)$ ms. (c) $\tau_{s3} \in [320, 400]$ ms. Grey area indicates the stable region calculated by the mean values of the control model parameters. In the figures, individual dot represents each subject experiment test. "×", "□","⋆", "○" and "◇" marks indicate subjects A to E, respectively. Blue and red marks indicate the stable and unstable parameters points, respectively. Similar to Fig. 11, the shaded areas are obtained by using the mean values of the control model parameters and for a particular subject, the stability is determined by using the control model parameters of that subject. Therefore, it is possible that red marks are located inside the shared areas.

D. Discussions

From Table I, the value of gain k_{b1} is much larger than that of k_{b3} for the upper-body roll angle φ_h. The angular rate gains k_{b2} and k_{b4} are within a similar range. Considering the magnitudes of φ_b, φ_h and their derivatives, the dominating term of (7) is the first one, that is, $k_{b1}\varphi_b$. This implies that the roll angle φ_b plays a more important role for balancing the platform than φ_h does. From Table II, the values of time delays τ_3 and τ_4 are (around 50 and 100 ms) larger respectively than those of τ_1 and τ_2. A possible explanation of these differences is that the human sensorimotor mechanism for steering actuation has a slower response than that of the body movement. This is consistent with the results reported in [42].

To observe the influence of steering delays on τ_1 and τ_2, Fig. 13 illustrates the stable regions in the τ_1-τ_2 plane under four different pairs of (τ_{s3}, τ_{s4}): $(200, 160)$, $(250, 210)$, $(300, 260)$ and $(350, 310)$ ms, respectively. We choose these pairs of (τ_{s3}, τ_{s4}) values because the starting pair is around $\tau_s = 0$. From these plots, the stable region is enlarged for

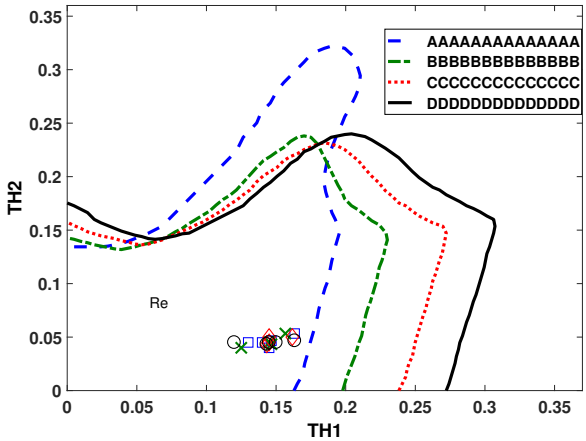

Fig. 13. Stable regions under under varying τ_1 and τ_2 with different delays τ_{s3} and τ_{s4}. The stable region is marked with $\mathrm{Re}(\lambda_0) < 0$. Blue "□", green "×", red "◇", and black "○" marks indicate the estimated mean values of (τ_1, τ_2) for each subject under these four pairs of time delay combinations τ_{s3}/τ_{s4}, respectively.

the large values of (τ_{s3}, τ_{s4}). The maximum value of τ_1 has increased almost around 50 ms for each incremental pair of (τ_{s3}, τ_{s4}) but the maximum values of τ_2 do not change significantly under varying (τ_{s3}, τ_{s4}). The identified values for τ_1 and τ_2 listed in Table II all fall into the stable regions and indeed these values do not change much when the steering delay τ_s is introduced in experiments. This could imply that the human riders prefer to use and adopt faster steering actions, rather than body movement, to respond the time delays produced by the actuator. This observation is consistent with the sensitivity analysis reported in [30].

The work in this study has several limitations. The model (6) includes only the dependency on bikebot and upper-body roll angles and their derivatives and some other factors are neglected, such as the possible influence of the steering action on torque u_h. We only recruited experienced bicycle riders as the subjects and it is not clear whether the presented results can be extended and applied to other types of bicycle riders. Moreover, the results do not include detailed stability analysis of the influence of bikebot velocity. Finally, this paper does not consider and discuss how to tune and adapt the human motor skills through the physical rider-bikebot interactions. Some preliminary results are reported in [43] and we will report the new developments in future publications.

VI. Conclusion

This paper presented the human balance control and stability analysis of the rider-bicycle systems. We first presented a rider-bikebot dynamic model. Inspired by the experimental data and the postural stance balance model, we proposed new PD-like feedback models with time delays for the human body movement and steering control for bicycle riding. The riding experiments with visual feedback and actuation perturbations were then conducted. We discussed the stability analysis of the rider-bicycle system and presented the influence of the model parameters, including the physical parameters, control gains and time delays, on the system stability. The results were also used to interpret the human balance capability and to compare with stance balance and balancing stationary bicycles that were reported previously. The work presented in this paper can serve as a foundation for the human balance motor skill tuning and developing bicycle/motorcycle riding assistive systems.

References

[1] P. Paoletti and L. Mahadevan, "Balancing on tightropes and slacklines," *J. R. Soc. Interface*, vol. 9, pp. 2097–2108, 2012.

[2] T. Insperger and J. Milton, "Sensory uncertainty and stick balancing at the fingertip," *Biol. Cybern.*, vol. 108, pp. 85–101, 2014.

[3] A. D. Goodworth and R. J. Peterka, "Influence of bilateral vestibular loss on spinal stabilization in humans," *J. Neurophysiol.*, vol. 103, pp. 1978–1987, 2010.

[4] J. T. Bingham and L. H. Ting, "Stability radius as a method for comparing the dynamics of neuromechanical systems," *IEEE Trans. Biomed. Eng.*, vol. 21, no. 5, pp. 840–848, 2013.

[5] D. Hajdu, J. Milton, and T. Insperger, "Extension of stability radius to neuromechanical systems with structured real perturbations," *IEEE Trans. Biomed. Eng.*, vol. 24, no. 11, pp. 1235–1242, 2016.

[6] J. R. Chagdes, S. Rietdyk, J. M. Haddad, H. N. Zelaznik, and A. Raman, "Dynamic stability of a human standing on a balance board," *J. Biomech.*, vol. 46, pp. 2593–2602, 2013.

[7] A. H. Snijders and B. R. Bloem, "Cycling for freezing of gait," *New Engl. J. Med.*, vol. 362, p. e46, 2010.

[8] M. Stamelou, M. Kojovic, M. J. Edwards, and K. P. Bhatia, "Ability to cycle despite severe freezing of gait in atypical Parkinsonism in Fahr's syndrome," *Mov. Disord.*, vol. 26, no. 11, pp. 2141–2142, 2011.

[9] A. H. Snijders, I. Toni, E. Růžička, and B. R. Bloem, "Bicycling breaks the ice for freezers of gait," *Mov. Disord.*, vol. 26, no. 3, pp. 367–371, 2011.

[10] C.-G. Song, J.-Y. Kim, and N.-G. Kim, "A new postural balance control system for rehabilitation training based on virtual cycling," *IEEE Trans. Inform. Technol. Biomed.*, vol. 8, no. 2, pp. 200–207, 2004.

[11] K. J. Åström, R. E. Klein, and A. Lennartsson, "Bicycle dynamics and control," *IEEE Control Syst. Mag.*, vol. 25, no. 4, pp. 26–47, 2005.

[12] J. Meijaard, J. Papadopoulos, A. Ruina, and A. Schwab, "Linearized dynamics equations for the balance and steer of a bicycle: A benchmark and review," *Proc. Royal Soc. A*, vol. 463, pp. 1955–1982, 2007.

[13] J. Moore and M. Hubbard, "Parametric study of bicycle stability (P207)," in *The Engineering of Sport 7*, M. Estivalet and P. Brisson, Eds. Springer-Verlag, 2008, vol. 2, pp. 311–318.

[14] J. D. G. Kooijman, J. Merjaard, J. M. Papadopoulos, A. Ruina, and A. Schwab, "A bicycle can be self-stable without gyroscopic or caster effects," *Science*, vol. 332, pp. 339–342, 2011.

[15] J. D. G. Kooijman and A. L. Schwab, "A review on bicycle and motorcycle rider control with a perspective on handling qualities," *Veh. Syst. Dyn.*, vol. 51, no. 11, pp. 1722–1764, 2013.

[16] A. D. Goodworth and R. J. Peterka, "Contribution of sensorimotor integration to spinal stabilization in humans," *J. Neurophysiol.*, vol. 102, pp. 496–512, 2009.

[17] D. Soudbakhsh, Y. Zhang, and J. Yi, "Stability analysis of human balance control of stationary bicycles," in *Proc. Amer. Control Conf.*, Montreal, Canada, 2012, pp. 2755–2760.

[18] J. Yi, D. Soudbakhsh, Y. Zhang, and Y. Zhang, "Why some Parkinson's disease patients cannot stand or walk but can ride a bicycle – A control system-based analysis," in *Proc. ASME Dyn. Syst. Control Conf.*, Ft. Lauderdale, FL, 2012, article # DSCC2012-8735.

[19] R. A. Hess, "Simplified approach for modelling pilot pursuit control behaviour in multi-loop flight control tasks," *Proc. IMechE Part G: J. Aero. Eng.*, vol. 220, no. G2, pp. 85–102, 2006.

[20] R. A. Hess, J. K. Moore, and M. Hubbard, "Modeling the manually controlled bicycle," *IEEE Trans. Syst., Man, Cybern. A*, vol. 42, no. 3, pp. 545–557, 2012.

[21] J. K. Moore, "Human control of a bicycle," Ph.D. dissertation, Dept. Mech. Aero. Eng., Univ. Calif. Davis, Davis, CA, 2012.

[22] S. M. Cain, "An experimental investigation of human/bicycle dynamics and rider skill in children and adults," Ph.D. dissertation, Dept. Biomed. Eng., Univ. Michigan, Ann Arbor, MI, 2013.

[23] Y. Zhang, F. Liu, M. Trkov, and J. Yi, "Rider/bicycle pose estimation with integrated IMU/seat force sensor measurements," in *Proc. IEEE/ASME Int. Conf. Adv. Intelli. Mechatronics*, Kaohsiung, Taiwan, 2012, pp. 604–609.

[24] R. Sipahi and N. Olgac, "Complete stability robustness of third-order LTI multiple time-delay systems," *Automatica*, vol. 41, no. 8, pp. 1413–1422, 2005.

[25] K. Gu, S. I. Niculescu, and J. Chen, "On stability crossing curves for general systems with two delays," *J. Math. Analy. App.*, vol. 311, no. 1, pp. 231–253, 2005.

[26] R. Sipahi, S.-I. Niculescu, C. T. Abdallah, W. Michiels, and K. Gu, "Stability and stabilization of systems with time delay," *IEEE Control Syst. Mag.*, vol. 31, no. 1, pp. 38–65, 2011.

[27] R. Sipahi and I. I. Delice, "Advanced clustering with frequency sweeping methodology for the stability analysis of multiple time-delay systems," *IEEE Trans. Automat. Contr.*, vol. 56, no. 2, pp. 467–472, 2011.

[28] Q. Gao and N. Olgac, "Stability analysis for LTI systems with multiple time delays using the bounds of its imaginary spectra," *Syst. Contr. Lett.*, vol. 102, pp. 112–118, 2017.

[29] T. Vyhlídal and P. Zítek, "Quasipolynomial mapping based rootfinder for analysis of time delay systems," *IFAC Proc. Vol.*, vol. 36, no. 19, pp. 227–232, 2003.

[30] P. Wang and J. Yi, "Balance equilibrium manifold and control of rider-bikebot systems," in *Proc. Amer. Control Conf.*, Boston, MA, 2016, pp. 2168–2174.

[31] ——, "Dynamic stability of a rider-bicycle system: Analysis and experiments," in *Proc. Amer. Control Conf.*, Chicago, IL, 2015, pp. 1161–1166.

[32] Y. Zhang, P. Wang, J. Yi, D. Song, and T. Liu, "Stationary balance control of a bikebot," in *Proc. IEEE Int. Conf. Robot. Autom.*, Hong Kong, China, 2014, pp. 6706–6711.

[33] Y. Zhang, K. Chen, and J. Yi, "Rider trunk and bicycle pose estimation with fusion of force/inertial sensors," *IEEE Trans. Biomed. Eng.*, vol. 60, no. 9, pp. 2541–2551, 2013.

[34] J. Yi, D. Song, A. Levandowski, and S. Jayasuriya, "Trajectory tracking and balance stabilization control of autonomous motorcycles," in *Proc. IEEE Int. Conf. Robot. Autom.*, Orlando, FL, 2006, pp. 2583–2589.
[35] J. Yi, Y. Zhang, and D. Song, "Autonomous motorcycles for agile maneuvers: Part I: Dynamic modeling," in *Proc. IEEE Conf. Decision Control*, Shanghai, China, 2009, pp. 4613–4618.
[36] Y. Zhang, J. Li, J. Yi, and D. Song, "Balance control and analysis of stationary riderless motorcycles," in *Proc. IEEE Int. Conf. Robot. Autom.*, Shanghai, China, 2011, pp. 3018–3023.
[37] Y. Tanaka and T. Murakami, "A study on straight-line tracking and posture control in electric bicycle," *IEEE Trans. Ind. Electron.*, vol. 56, no. 1, pp. 159–168, 2009.
[38] Y. Zhang, K. Chen, and J. Yi, "Rider/bicycle pose estimation with IMU/seat force measurements," in *Proc. Amer. Control Conf.*, Washington DC, 2013, pp. 2846–2851.
[39] D. M. Wolpert, R. C. Miall, and M. Kawato, "Internal models in the cerebellum," *Trends Cognit. Sci.*, vol. 2, no. 9, pp. 338–347, 1998.
[40] M. J. Wagner and M. A. Smith, "Shared internal models for feedforward and feedback control," *J. Neurosci.*, vol. 42, pp. 10 663–10 673, 2008.
[41] http://www.cak.fs.cvut.cz/algorithms/qpmr.
[42] A. van Lunteren and H. G. Stassen, "On the influence of drugs on the behavior of a bicycle rider," in *Proc. 6th Ann. Conf. Manual Control*, Wright-Patterson AFB, OH, 1970, pp. 419–437.
[43] P. Wang and J. Yi, "Balance performance tuning of rider-bikebot interactions," in *Proc. Amer. Control Conf.*, Milwaukee, WI, 2018, pp. 1333–1338.

Jingang Yi (S'99-M'02-SM'07) received the B.S. degree in electrical engineering from Zhejiang University, Hangzhou, China, in 1993, the M.Eng. degree in precision instruments from Tsinghua University, Beijing, China, in 1996, and the M.A. degree in mathematics and the Ph.D. degree in mechanical engineering from the University of California, Berkeley, CA, USA, in 2001 and 2002, respectively.

He is currently an Associate Professor of Mechanical Engineering at Rutgers University. His research interests include autonomous robotic systems, dynamic systems and control, mechatronics, automation science and engineering, with applications to biomedical systems, civil infrastructure and transportation systems.

Dr. Yi is a Fellow of the American Society of Mechanical Engineers (ASME). He was a recipient of the 2010 U.S. NSF CAREER Award. He has co-authored papers that have been awarded several best papers in the IEEE TRANSACTIONS ON AUTOMATION SCIENCE AND ENGINEERING, IEEE/ASME AIM, ASME DSCC, and IEEE ICRA. He currently serves as an Associate Editor of the IEEE TRANSACTIONS ON AUTOMATION SCIENCE AND ENGINEERING IEEE/ASME TRANSACTIONS ON MECHATRONICS, IEEE ROBOTICS AND AUTOMATION LETTERS, *IFAC Journal Mechatronics*, *International Journal of Intelligent Robotics and Applications*, and the IEEE Robotics and Automation Society Conference Editorial Board (since 2008). He also served as a Guest Editor of the IEEE TRANSACTIONS ON AUTOMATION SCIENCE AND ENGINEERING in 2009, *International Journal of Intelligent Robotics and Applications* in 2017, and an Associate Editor of *IFAC Control Engineering Practice* (2013-2017), *ASME Journal of Dynamic Systems, Measurement and Control* (2014-2018), the ASME Dynamic Systems and Control Division Conference Editorial Board from 2008 to 2010.

Pengcheng Wang (S'13) received the B.S. degree in automation and the M.S. degree in robotics, both from Nankai University, Tianjin, China, in 2009 and 2012, respectively, and the Ph.D. degree in mechanical engineering at Rutgers University, Piscataway, NJ, USA in 2018. He is currently a research engineer at the Innovation Academy for Microsatellites of Chinese Academy of Sciences, Shanghai, China.

His current interests include dynamics modeling, orbital and attitude control systems (AOCS), modeling and control of Human Machine Interactions (HMI) and control of underactuated robotics systems including single-track vehicles and cranes.

Tao Liu (M'08-SM'15) received the B.S. degree in mechanical engineering from the Harbin University of Science and Technology, Harbin, China in 2001, M. Eng. degree in mechanical engineering from the Harbin Institute of Technology, Harbin, China, in 2003 and the D.Eng. from Kochi University of Technology, Kochi, Japan, in 2006. He was an Assistant Professor in the Department of Intelligent Mechanical Systems Engineering, Kochi University of Technology, Japan, from 2009 to 2013. He is currently a Professor of the State Key Laboratory of Fluid Power Transmission and Control and School of Mechanical Engineering, Zhejiang University, Hangzhou, China. His current research interests include wearable sensor systems, rehabilitation robots, biomechanics, and human motion analysis.

Dr. Liu is an inventor of one Japanese patent about wearable sensors for gait analysis that has been successfully commercialized. He was a recipient of the Japan Society of Mechanical Engineers (JSME) Encouragement Prize (2010).